RESEARCH REPORT

THE EFFECT OF ALLOY COMPOSITION ON THE MECHANISM OF STRESS-CORROSION CRACKING OF TITANIUM ALLOYS IN AQUEOUS ENVIRONMENTS

to

NATIONAL AERONAUTICS AND
SPACE ADMINISTRATION
Contract No. NASW-2242

February 1972

Battelle
Columbus Laboratories

QUARTERLY PROGRESS REPORT

(September 11, 1971 - December 11, 1971)

on

THE EFFECT OF ALLOY COMPOSITION ON THE MECHANISM OF STRESS-CORROSION CRACKING OF TITANIUM ALLOYS IN AQUEOUS ENVIRONMENTS

to

NATIONAL AERONAUTICS AND
SPACE ADMINISTRATION
Contract No. NASW-2242

February 1972

by

J. D. Boyd, D. N. Williams, R. A. Wood,
and R. I. Jaffee

BATTELLE
Columbus Laboratories
505 King Avenue
Columbus, Ohio 43201

TABLE OF CONTENTS

THE EFFECT OF ALLOY COMPOSITION ON THE MECHANISM OF STRESS-CORROSION CRACKING OF TITANIUM ALLOYS IN AQUEOUS ENVIRONMENTS

by

J. D. Boyd, D. N. Williams, R. A. Wood,
and R. I. Jaffee

INTRODUCTION

This research program is concerned with the effects of alloy composition on the aqueous stress corrosion of titanium alloys. Emphasis is being placed on determining the interrelations among the composition, phase structure, and deformation and fracture properties of the alpha phase in susceptible alpha-beta alloys. The program is divided into two parts. The first consists of evaluating the aqueous stress-corrosion susceptibility of a series of alloys that contain various alpha-soluble elements. The second consists of an investigation of the metallurgical aspects of the mechanism of aqueous stress-corrosion cracking. During the second quarter of the contract period, work has progressed simultaneously on both parts of the research program. Significant accomplishments are summarized below.

EFFECTS OF ALLOY COMPOSITION ON SUSCEPTIBILITY

Materials Preparation

The seven 5.4-kilogram ingots purchased from Titanium Metals Corporation were press forged to 5.6 to 6.1-cm thickness at 1150 C. The major billet surfaces were surface ground to remove about 2.5 mm per surface to eliminate contamination and defects resulting from forging. Billets were next hot rolled to both 6.4 and 3.2 mm plate and sheet, respectively, using the schedules given in Table 1. Beta-transus temperatures were determined metallographically with the results given in Table 2. Coupons will be cut from these flat-rolled products for the procedures of heat treatment, surface conditioning, sample preparation, and testing, as in prior work. The solution-annealing temperatures to be used for the alloys are given in Table 2 also.

The 6-cm-thick rolled plate of Ti-4Al-3Mo-1V alloy for use in studies of the effects of thickness on stress-corrosion behavior was cut into coupons of various thicknesses as shown in Figure 1. Coupons 6.4 mm thick from section A in the diagram were solution annealed for 3.6×10^3 seconds at 900 C, furnace cooled to 650 C at 38 C/3.6×10^3 seconds, held at 650 C for 3.6×10^3 seconds and air cooled to room temperature. Tensile data generated from these annealed samples (a) and from the as-received plate (b) are given in Table 3. The strengths of both annealed and as-received plate are quite low compared with the Ti-4Al-3Mo-1V material previously used on this program

TABLE 1. FABRICATION SCHEDULE FOR EXPERIMENTAL ALLOYS OBTAINED FOR FOURTH-YEAR STUDY [5.4-KG (~12 POUND) INGOTS AT 10.5 CM (~4.1 IN.) DIAMETER]

Alloy	Composition[a], weight percent	1150 C (2100 F) Press Forging[b]		Cross Rolling to 18-Cm (~7.1 in.) Width		Direct Rolling Temp, C (F)			Fabrication Rating
		Thickness, cm (in.)	Rating	Temp, C (F)	Thickness, cm (in.)	To 1.3 Cm (~0.5 In.)[c] Thick	To 0.6 Cm (~0.24 In.)[d] Thick	To 0.3 Cm (~0.12 In.) Thick	
4621	Ti-5Al-6Sn-1.5Mo-0.5V	5.9 (2.32)	Good	955 (1750)	3.8 (~1.5)	904-927 (1660-1700)	904 (1660)	893 (1640)	Good
4622	Ti-5Al-6Ga-1.5Mo-0.5V	6.1 (2.40)	Good	955 (1750)	4.2 (1.65)	904-955 (1660-1750)	904 (1660)	893 (1640)	Good to Fair[f]
4623	Ti-5Al-6In-1.5Mo-0.5V	5.9 (2.32)	Good	955 (1750)	3.8 (~1.5)	904-927 (1660-1700)	904 (1660)	893 (1640)	Good
4624	Ti-5Al-10Zr-1.5Mo-0.5V	5.6 (2.20)	Good	927-955 (1700-1750)	3.2 (1.26)	904-927 (1660-1700)	904 (1660)	893 (1640)	Good
4625	Ti-6Al-5Ta-1.5Mo-0.5V	5.9 (2.32)	Good	927-955 (1700-1750)	3.2 (1.26)	904-927 (1660-1700)	904 (1660)	893 (1640)	Good
4626	Ti-6Al-3Cb-1.5Mo-0.5V	5.6 (2.20)	Good	927-955 (1700-1750)	3.2 (1.26)	904-927 (1660-1700)	904 (1660)	893 (1640)	Good
4627	Ti-8Al binary	5.6 (2.20)	Good	927-955 (1700-1750)	3.2 (1.26)	927 (1700)[e]	927 (1700)	927 (1700)	Fair to Poor[g]

(a) 0.10 percent nominal oxygen (to be analyzed).
(b) Draw-down-type forging (not upset).
(c) All material subsequently rolled to 1.3-cm (~0.5 in.) thickness with appropriate intermediate conditioning.
(d) One-third length of 0.6-cm (~0.24 in.) thick plates subsequently rolled to 0.3-cm (~0.12 in.) sheet.
(e) Severe cracking at 1.5-cm (~0.6 in.) thickness. All surfaces conditioned by extensive machining.
(f) Many edge cracks. Balance was good material.
(g) Very stiff material. The alloy cracked extensively during hot rolling.

TABLE 2. BETA-TRANSUS AND SOLUTION-ANNEALING TEMPERATURES USED FOR ALLOYS OF FOURTH-YEAR STUDY[a]

Alloy	Composition, weight percent	Test-Temperature Range, 10 C (50 F) Increments	Beta Transus Temperature, C (F)	Solution-Annealing Temperature, C (F)[a]
4621	Ti-5Al-6Sn-1.5Mo-0.5V	870-1010 (1600-1850)	971 (1780)	943 (1730)
4622	Ti-5Al-6Ga-1.5Mo-0.5V	870-1010 (1600-1850)	971 (1780)	943 (1730)
4623	Ti-5Al-6In-1.5Mo-0.5V	870-1010 (1600-1850)	960 (1760)	932 (1710)
4624	Ti-5Al-10Zr-1.5Mo-0.5V	870-1010 (1600-1850)	932 (1710)	904 (1660)
4625	Ti-6Al-5Ta-1.5Mo-0.5V	870-1010 (1600-1850)	966 (1770)	943 (1730)
4626	Ti-6Al-3Cb-1.5Mo-0.5V	870-1010 (1600-1850)	971 (1780)	943 (1730)
4627	Ti-8Al binary	927-1093 (1700-2000)	1050 (1925)[c]	900 (1650)[c]

(a) Solution-annealing temperatures expected to be used [about 10 C (50 F) below beta-transus temperature].
(b) Previous Ti-8Al material was annealed at 900 C (1650 F) for 24 hours.
(c) Previous ingot of Ti-8Al alloy had a transus temperature of 1025 C (1875 F).

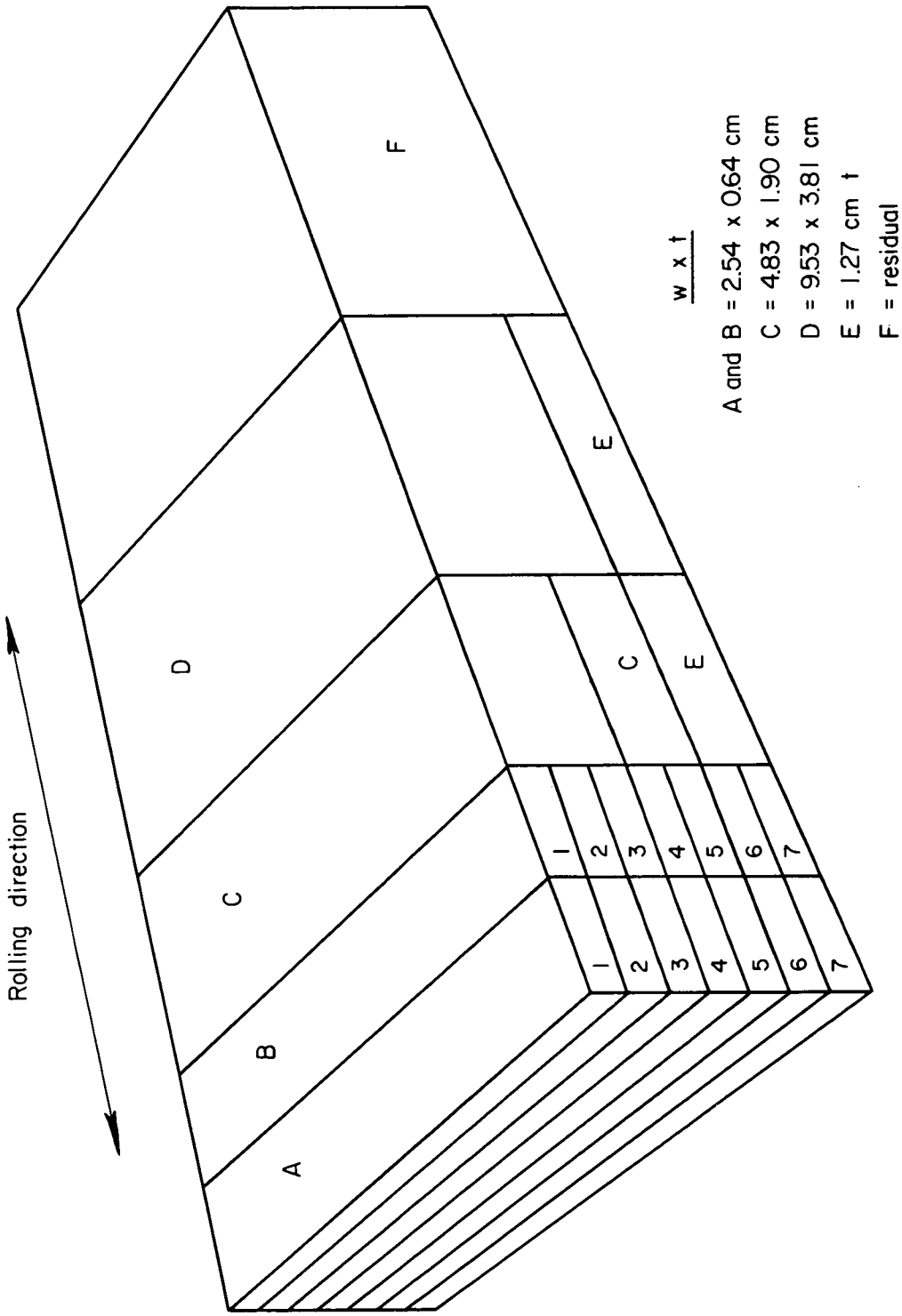

FIGURE 1. COUPON-CUTTING DIAGRAM OF 6-CM-THICK, Ti-4Al-3Mo-IV PLATE

TABLE 3. ROOM-TEMPERATURE TENSILE PROPERTIES OF Ti-4Al-3Mo-IV ALLOY PLATE (6-CM THICKNESS) AS RECEIVED AND AS SOLUTION ANNEALED (0.005 IN./IN./MIN ė)

Sample	Test Direction[a]	0.2% Offset Yield Strength, N/m^2 (ksi)	Ultimate Strength, N/m^2 (ksi)	Ductility, percent	
				Elongation	Reduction in Area
A-1[b, c, d, f]	Transverse	710 (103)	786 (114)	12	23
A-4[b, c, d, f]	Transverse	662 (96)	751 (109)	11	25
B-1[b, d, f]	Transverse	772 (112)	862 (125)	10	20
B-4[b, d, f]	Transverse	710 (103)	813 (118)	8	18
70[e]	Longitudinal	641 (93)	786 (114)	17	28
	Longitudinal	641 (93)	765 (111)	17	35
	Transverse	786 (114)	820 (119)	18	47
	Transverse	793 (115)	820 (119)	15	46
41[e, f]	Transverse	834 (121)	882 (128)	17	39
	Transverse	848 (123)	896 (130)	18	40

(a) With respect to rolling direction.
(b) 0.6-cm (~0.24 in.) thick samples machined from 6-cm (2.36 in.) plate.
(c) Solution annealed for 1 hour at 900 C (1650 F), furnace cooled to 650 C (1200 F) at 38 C/hour (100 F/hour), held 1 hour at 650 C (1200 F), and air cooled to room temperature.
(d) Samples A-1 and B-1 are from plate surface; samples A-4 and B-4 are from plate center (see Figure 1).
(e) 0.3-cm (~0.12 in.) thick samples machined from 0.3-cm sheet.
(f) Commercially produced material.

(data are given in Table 3 for comparison). Further, material from the center of the thick plate (A-4, B-4) has lower strength than surface material (A-1, B-1). Metallographic examination shows that the microstructures are quite acicular and coarse, which indicates a beta fabrication schedule for the plate rolled to the 6-cm thickness (the solution annealing treatment does not alter the microstructure greatly). Plate-center microstructures are somewhat coarser than plate surfaces, as might be expected. The significance of the low strength and microstructural characteristics of this material relative to the effect-of-thickness experimental success (in terms of meaningful results) is an unknown factor at this time.

METALLURGICAL MECHANISMS OF STRESS-CORROSION CRACKING

Background

It is well established that the resistance of titanium aluminum-base alloys to subcritical crack growth in aqueous environments is drastically reduced by the precipitation of long-range-ordered Ti_3Al particles in the alpha phase. This phenomenon was demonstrated first by Lane and Cavallaro[1], and subsequently by several other workers[2-7]. The specific effect of the Ti_3Al particles on the mechanism of subcritical crack growth is thought to be a combination of the following factors:

(1) The coherent, ordered precipitates promote nonhomogeneous, planar slip. This slip mode generally occurs in alloys hardened by coherent precipitates because the areal fraction of precipitate in a given slip plane decreases with passage of each dislocation. Hence, it requires a lower stress to move dislocations in an active slip plane than to initiate slip in an area where the particles have not been previously sheared. Consequently, the slip bands tend to be narrow and widely spaced, and to have large shear displacements. The ordered nature of the particles causes the dislocations to move as pairs of perfect $\frac{a}{3}[11\bar{2}0]$ dislocations separated by a strip of antiphase boundary, which makes it difficult for obstacles to be bypassed by cross slip. The result is that long coplanar pileups of dislocations form at obstacles, and large shear displacements occur at free surfaces. The former effect produces high normal stresses which could cause cleavage, and the latter exposes large areas of bare metal to the environment which could act as active anodic sites.

(2) The slip bands have a higher chemical potential than the undeformed material. This is a consequence of the increased density of antiphase boundary in the sheared particles, their decreased size (Gibbs-Thompson Effect), and the tendency toward particle re-solution in the slip bands[6, 8]. The enhanced chemical potential of the slip bands caused by the sheared Ti_3Al particles is expected to increase the rate of any electrochemical reaction occurring at surface slip steps.

(3) Ti_3Al particles make an alloy intrinsically more brittle[3, 8, 9].

Recently it has been demonstrated by Cavallaro and Wilcox[5] that the degree of embrittlement, in air as well as in salt water, is a function of the size distribution of the Ti_3Al particles. Specifically, they showed that the salt-water fracture stress of Ti-7 weight percent Al initially decreases with aging time at 650 C, reaches a minimum value at approximately 3.6×10^5 seconds, and then increases. Extrapolating their data suggests that the salt-water fracture stress should be equal to the air value after approximately 3.6×10^6 seconds, aging at 650 C. They also demonstrated that the air fracture toughness (as given by the Charpy V-notch impact energy) has a similar dependence on aging time. Cavallaro and Wilcox did not determine the cause of this behavior, but Lütjering and Weissman[8] have studied this phenomenon in a series of alloys of slightly higher aluminum contents, and they ascribed the increased toughness to a change in the slip mechanism from particle shearing to particle bypass. When the bypass mechanism is operative, the dislocation debris which accumulates in the vicinity of the particles hardens the active slip planes, which favors the initiation of new slip planes, and results in a more homogeneous slip character. Lütjering and Weissman concluded that this type of slip character is associated with a homogeneous distribution of large (> 0.1 μm), widely-separated precipitates. Lütjering and Weissman did not consider the effects of slip character on stress-corrosion cracking, but it is clear that when the particle-bypass mechanism predominates, the detrimental effects of Ti_3Al particles described above are alleviated.

The objective of the present research is to investigate the effect of the size distribution of Ti_3Al particles on the susceptibility of titanium-aluminum-base alloys to subcritical crack growth in aqueous environments. Binary Ti-8Al is being used for most of the work since this alloy has been studied extensively during the earlier phases of this research program. Also, aging at a temperature just below the α - α + Ti_3Al phase boundary ought to produce a size distribution of Ti_3Al particles which gives the particle bypass mechanism and homogeneous slip, without the complication of precipitation during the quench from the aging temperature. Some of the experimental alloys described in the first section of this report are also being studied to determine the effect of various alpha-soluble elements (Ga, Sn, Zn, Cb, Ta) on the Ti_3Al size distribution. The general approach is to produce different Ti_3Al size distributions by isothermal aging treatments at various temperatures, and to characterize the particle-size distributions by transmission electron microscopy (usually imaging the particles in dark field using a $11\bar{2}0_{\alpha_2}$ reflection. The slip character is studied by means of transmission electron microscopy and high-resolution, two-stage surface replicas, and the tensile properties in air and salt water are determined by uniaxial tensile tests of sheet specimens 6.35×10^{-4} m thick.

Summary of Results

All specimens were solution treated 8.64×10^4 seconds at 900 C and water quenched. This heat treatment produced a microstructure consisting of large, equiaxed alpha grains (average grain diameter ≃60 μm. Transmission electron microscopy showed that the grains were essentially dislocation-free, and there was no evidence of ordering in the electron-diffraction patterns (Figure 2a).

The first aging treatment to be investigated was 3.6×10^5 seconds at 500 C. This treatment produced a fine dispersion of spherical Ti_3Al particles 2.5 to 5.0×10^{-9} m in diameter (Figure 2b). Since the precipitate coarsening rate at 500 C is

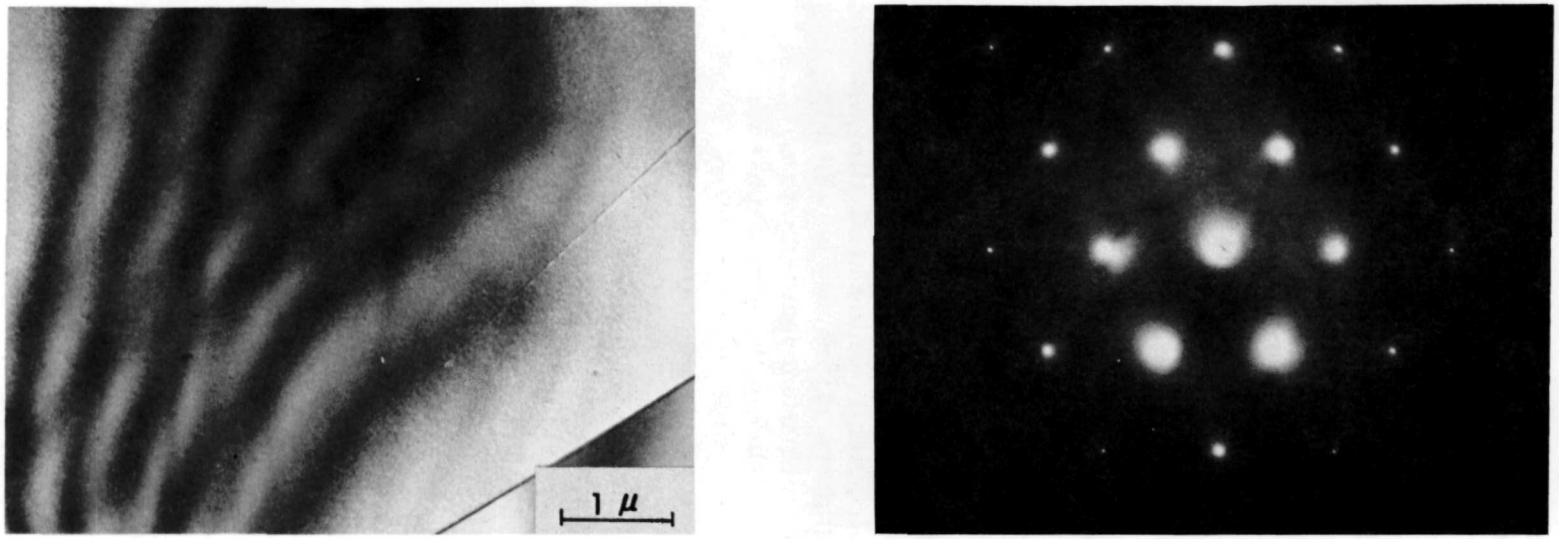

a. 24 Hours at 900 C, W.Q., $[0001]_\alpha$ Zone, Bright-Field Micrograph Showing Dislocation-Free Alpha Grain

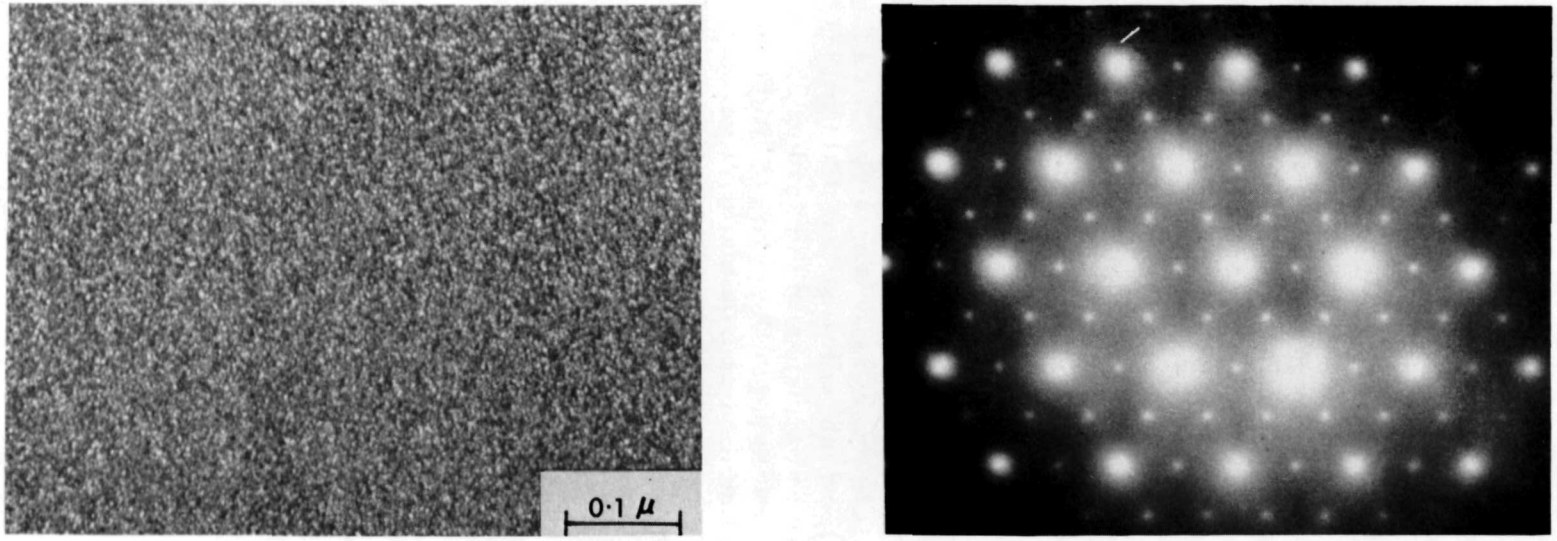

b. 24 Hours at 900 C, W.Q., + 100 Hours at 500 C, A.Q., $[0001]_\alpha$ Zone, Dark-Field Micrograph, $\bar{g} = 11\bar{2}0_{\alpha_2}$, Showing Ti_3Al Precipitates

FIGURE 2. MICROSTRUCTURES OF Ti-8Al

very low, this was the only aging time employed at 500 C. The stress-strain curves for specimens in the quenched as well as the quenched-and-aged conditions are shown in Figures 3(a) and 3(b), respectively. (The arrows indicate the strains at which the incremental tests were replicated). Specimens in the quenched condition exhibited an initial stage of rapid work hardening, followed by a sharply decreased rate of work hardening after approximately 1 percent plastic strain, tensile instability at approximately 8 percent strain, and fracture after approximately 14 percent elongation. Essentially identical behavior was observed for specimens deformed in air or salt water. By comparison, specimens in the aged condition showed distinct differences between the air and salt-water tests. In air, the aged specimens exhibited a sharp yield drop followed by an interval of negligible work hardening which ended after 2 to 4 percent plastic strain. Subsequently, the flow stress increased slowly to an ultimate stress slightly in excess of the upper yield stress, tensile instability began at 10 to 12 percent strain, and fracture occurred at approximately 18 percent elongation. The aged specimens exhibited the same yield and work-hardening characteristics in salt water as in air up to approximately 10 percent strain, at which point a through-thickness crack formed in the center of the specimen and propagated slowly across the breadth of the specimen. The average velocity of this slow crack growth was 7×10^{-5} m-sec^{-1}.

The slip character was distinctly nonhomogeneous for both heat treatments. However, the slip bands were somewhat straighter in the aged alloy than in the single-phase alloy. In the latter condition, a coarse, straight, slip band often spread into many fine wavy slip bands in the vicinity of obstacles such as grain boundaries or other slip bands (Figure 4a). This was observed much less frequently in the aged alloy (Figure 4b), which indicates that dislocations are much more rigorously confined to their original slip planes in the aged alloy. However, a prevalent feature was observed in specimens in the aged condition which was not found in the single-phase alloy. Beginning at approximately 4 percent strain, trench-like features were observed along slip steps in nearly half the grains examined. This feature can be identified by a black line adjacent to a white shadow (Figure 5). The shadows from the trenches were usually ragged, suggesting that the contours of the trenches were very irregular. A notable characteristic of the trenches was their specificity to a particular slip system in a given grain. For example, in grains deforming by multiple slip, the trenches could be found on nearly every slip band belonging to only one or perhaps two of the slip systems, but were not evident in the remaining systems in the grain (e.g., Figure 5b).

The dislocation substructures in deformed specimens correlated with the slip-line observations. In both quenched and quenched-and-aged specimens, the predominant slip systems were of the type $\frac{a}{3}\left\langle 11\bar{2}0\right\rangle\left\{1\bar{1}00\right\}$. However, in the aged specimens, the slip bands tended to be narrower, and more rigorously planar, with less cross slip, and less nonprism slip. Furthermore, the Ti_3Al particles in most slip bands were sheared so as to be no longer visible in dark field (Figure 6). This indicated that the long-range order of the particles in the slip bands no longer existed owing to a high density of slip-induced antiphase boundaries, or that the particles had redissolved.

The second aging temperature to be employed in this investigation was 650 C, which was selected because it was the aging temperature used by Cavallero and Wilcox. Aging up to 1.8×10^6 seconds at 650 C produced a homogeneous distribution of

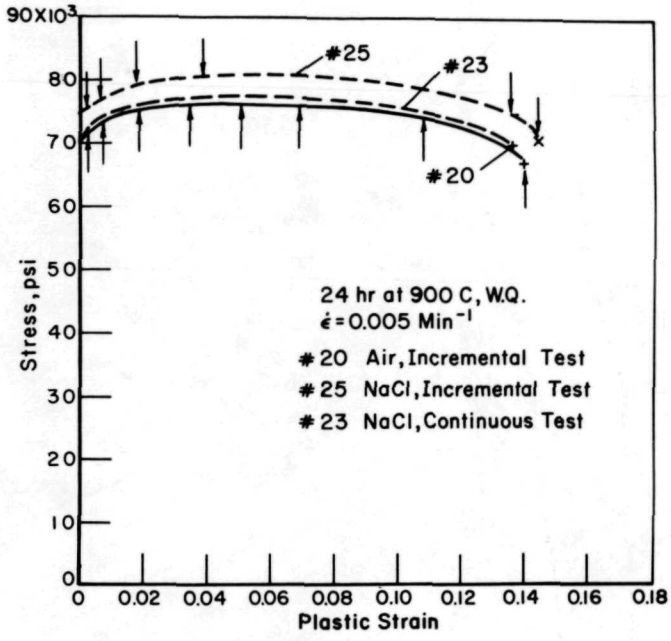

a. 24 Hours at 900 C, W.Q.

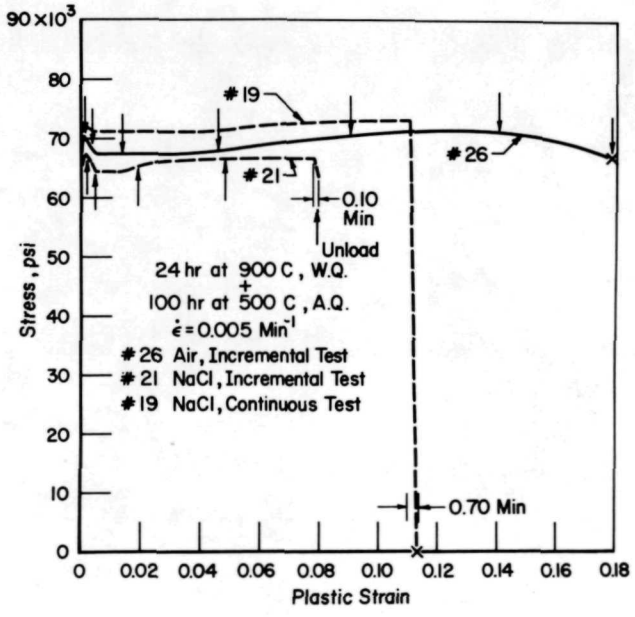

b. 24 Hours at 900 C, W.Q. + 100 Hours at 500 C, A.Q.

FIGURE 3. STRESS-STRAIN CURVES FOR Ti-8Al IN AIR AND IN SALT WATER ($\dot{\epsilon}$ = .005 min^{-1})

a. 24 Hours at 900 C, W.Q. (ϵ = .02)

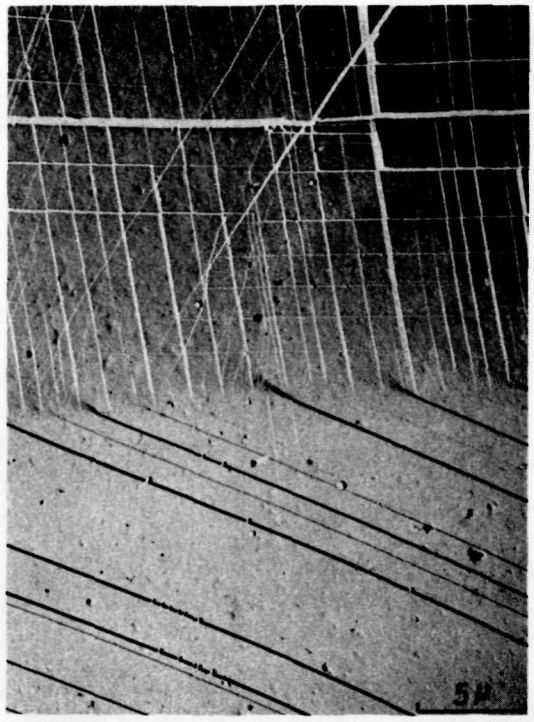

b. 24 Hours at 900 C, W.Q. + 100 Hours at 500 C, A.Q. (ϵ = .05)

c. 24 Hours at 900 C, W.Q. (Adjacent to Fracture)

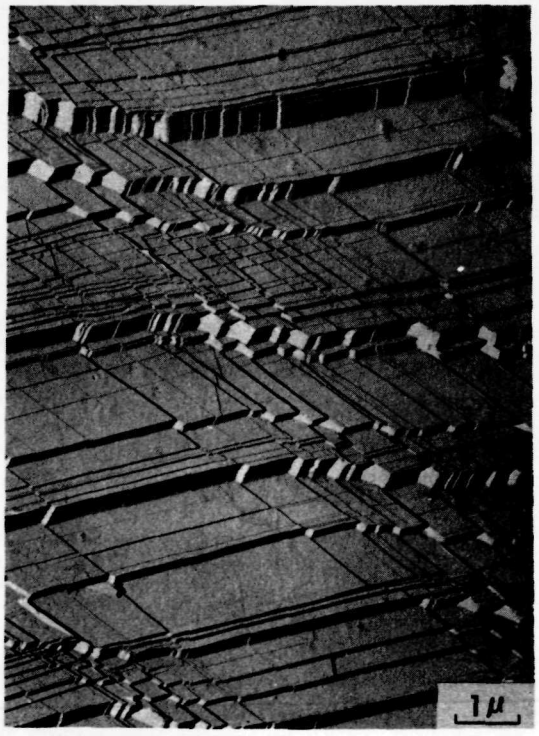

d. 24 Hours at 900 C, W.Q. + 100 Hours at 500 C, A.Q. (Adjacent to Fracture)

FIGURE 4. SURFACE SLIP LINES IN Ti-8Al

a. $\epsilon = 0.02$

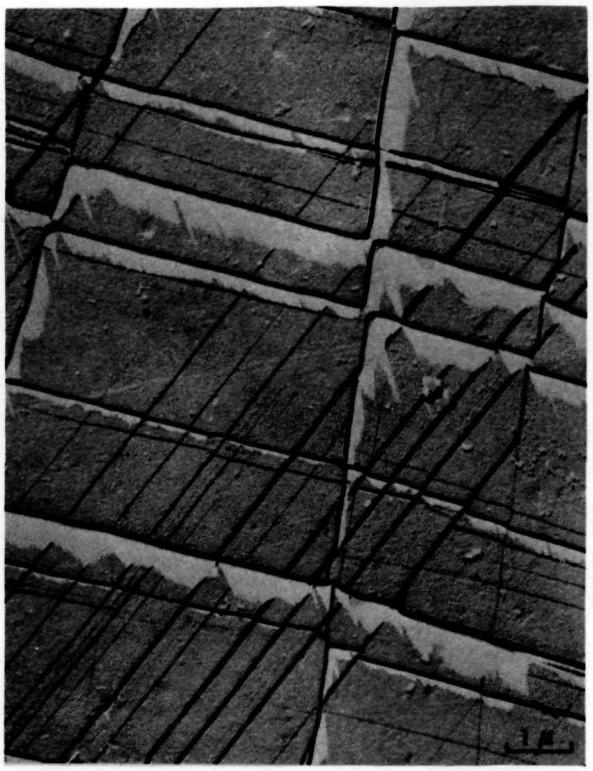

b. $\epsilon = 0.05$

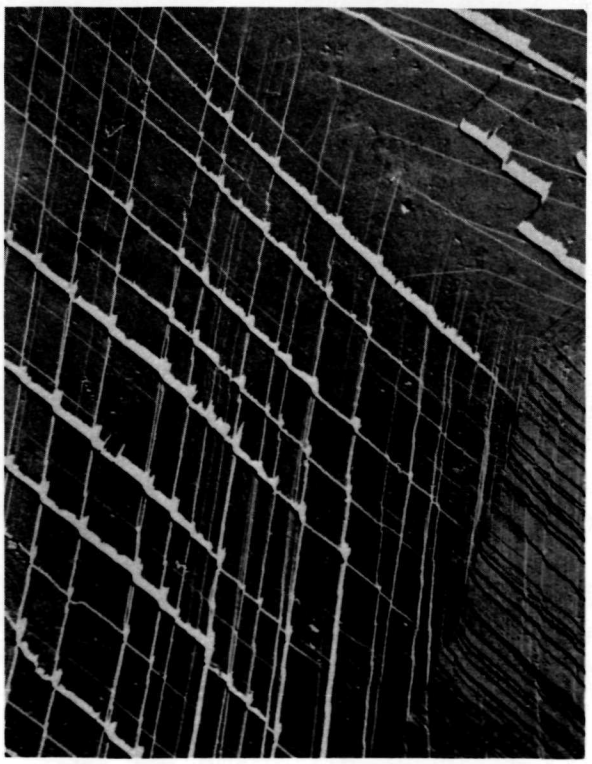

c. $\epsilon = 0.08$ (Cracking)

d. $\epsilon = 0.08$ (Cracking)

FIGURE 5. SURFACE SLIP LINES IN Ti-8Al HEAT TREATED 24 HOURS AT 900 C, W.Q. + 100 HOURS AT 500 C, A.Q., DEFORMED IN SALT WATER

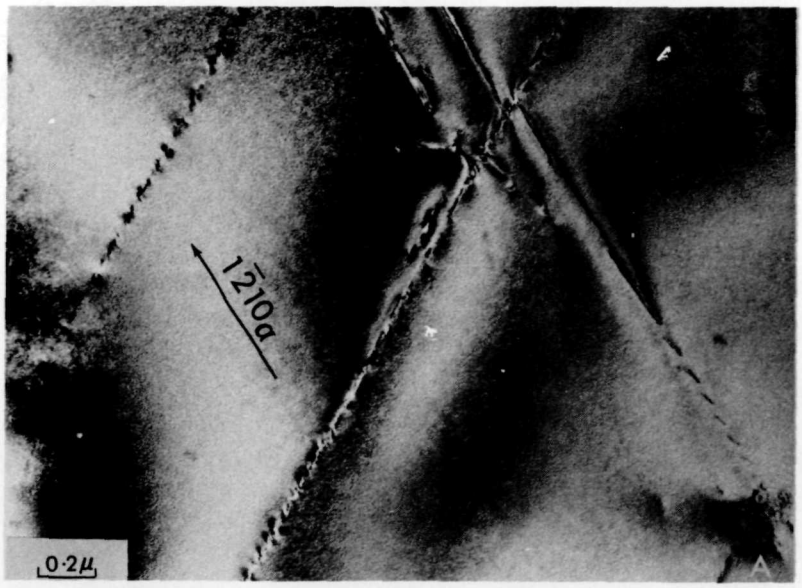

a. Shows $\{10\bar{1}0\}$ Slip Bands

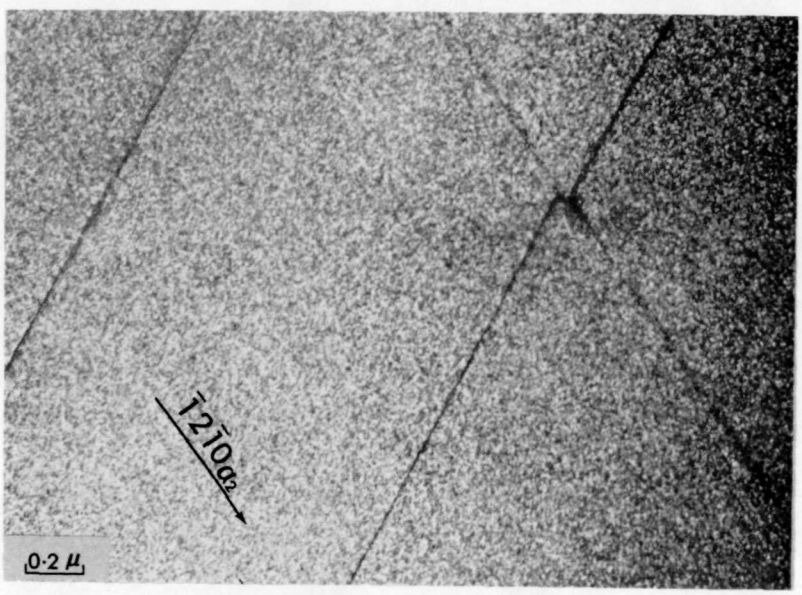

b. Dark-Field Micrograph of Same Area Showing Absence of Ti_3Al Precipitates in Slip Bands (Arrows Indicate Diffraction Vectors)

FIGURE 6. Ti-8Al HEAT TREATED 24 HOURS AT 900 C, W.Q. + 100 HOURS AT 500 C, A.Q.

Ti_3Al particles, with no tendency toward the ellipsoidal morphology which has been reported to occur at higher aging temperatures and in more concentrated alloys[3, 8]. Figure 7 shows that the precipitate size distribution produced by this heat treatment is such that the Ti_3Al particles are sheared by the glide dislocations. However, unlike the specimens aged at 500 C which showed a complete absence of precipitates in the slip bands (Figure 6), the larger precipitates which resulted from aging at 650 C (3 to 5 x 10^{-8} m), were still visible in the slip bands, although they were fragmented. Since the results of Cavallaro and Wilcox indicate an increase in salt-water fracture stress for aging times greater than 3.6×10^5 seconds at 650 C (for Ti7Al), it appears that the increased toughness in salt water is not associated with a transition in the slip mechanism from particle shearing to particle bypass.

It is suggested that the important event here is the destruction of the long-range order of the Ti_3Al precipitates in the active slip bands. When this occurs to a significant extent, the chemical potential of the surface slip steps is enhanced, as is the rate of the anodic reaction which occurs at freshly created slip steps. Without specifying the details of the anodic reaction or the exact mechanism of crack extension, it can be argued that a critical minimum rate for the anodic reaction must be exceeded for subcritical cracking to proceed. The degree to which the long-range order of the Ti_3Al particles is destroyed by slip (as indicated by their visibility in the slip bands) is a function of the size of the particles. Therefore, the chemical potential of surface slip steps, and, hence, the susceptibility to subcritical crack growth should decrease as the particle-size distribution coarsens. This hypothesis will be tested in two ways. First, the tensile properties of specimens aged for various times up to 3.6×10^6 seconds at 650 C will be determined in air and in salt water. It is expected that the plastic strain which occurs before the onset of subcritical cracking in salt water will increase with increasing mean particle size, until it is equal to the air value. A second test of the hypothesis is the appearance of trenches as revealed by surface replicas. It is felt that these features also indicate a high cehmical potential for the slip bands, and should appear less frequently with increasing mean particle size.

The final aging temperature which has been used in these studies is 700 C. This temperature was chosen in an attempt to obtain a lower density of particles and a larger particle size, in keeping with the Lütjering-Weissmann condition for the particle bypass mechanism. Figure 8 shows that the density of particles is indeed much less after aging 1.8×10^6 seconds, at 700 C, compared with the same time at 650 C, but the particles are still sheared. However, it is hoped that prolonged aging at 700 C will produce a sufficiently large particle size for the slip mechanism to be particle bypass. (Note that these results indicate that the α - α + Ti_3Al phase boundary given by Blackburn[10] is somewhat incorrect in the vicinity of 700 C and 8 weight percent aluminum. The phase boundary indicated by the results of Lütjering and Weissman appears to be correct.)

PLANS FOR FUTURE RESEARCH

Specimens of Ti-8Al will be aged for various times up to 3.6×10^6 seconds at 650 C, and their tensile properties determined in air and salt water. The morphology of the surface slip lines, in particular the appearance of trenches at the slip bands, will be correlated with the Ti_3Al size distribution.

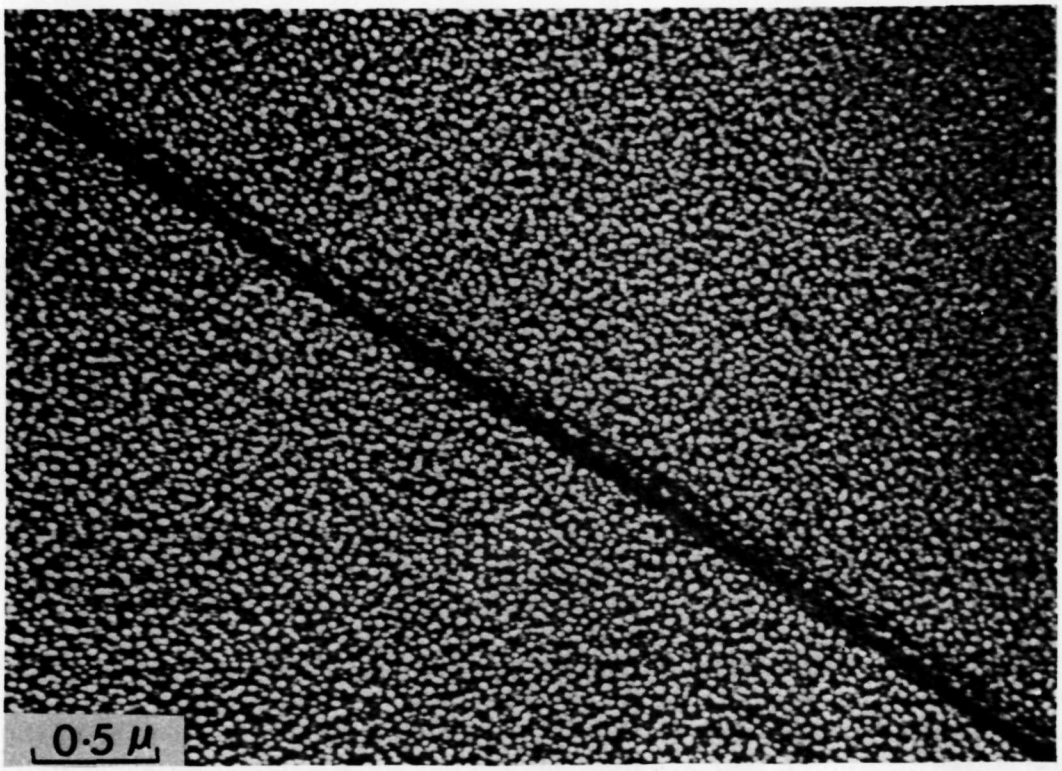

FIGURE 7. Ti-8Al AGED 500 HOURS AT 650 C (ϵ = .005) SHOWING SHEARED PARTICLES IN A SLIP BAND

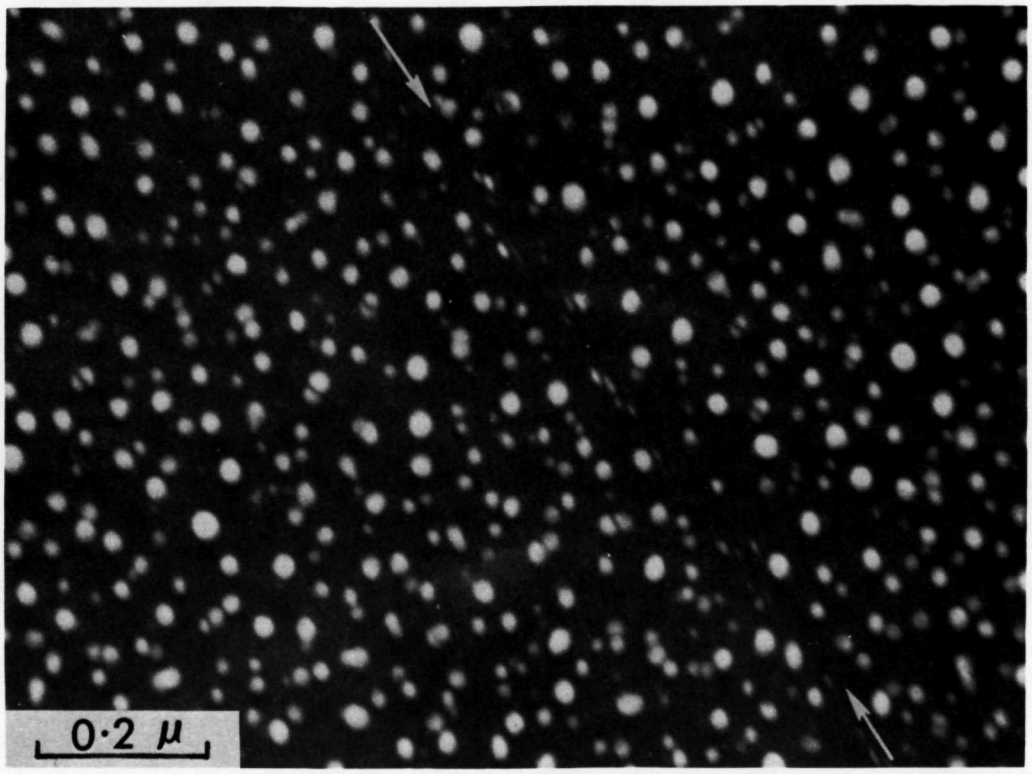

FIGURE 8. Ti-8Al AGED 500 HOURS AT 700 C (ϵ = .005) SHOWING SHEARED PARTICLES IN A SLIP BAND

Attempts will be made to obtain a size distribution of Ti_3Al precipitates which causes the glide dislocation to bypass the particles. This effort will consist of evaluating the effects of prolonged aging at 700 C, and of deformation prior to aging.

Selected alloys from the list in Table 1 will be studied by transmission electron microscopy to determine the effects of various alpha-soluble elements on the size distribution of Ti_3Al precipitates. Any alloy which has a Ti_3Al size distribution significantly different compared with that found in Ti-8Al will be subjected to further study to determine the slip character and the details of the dislocation-particle interaction.

REFERENCES

(1) I. R. Lane and J. L. Cavallaro, "Metallurgical and Mechanical Aspects of the Sea-Water Stress Corrosion of Titanium", in Applications Related Phenomena in Titanium Alloys, ASTM STP 432, 147 (1968).

(2) M. J. Blackburn and J. C. Williams, "Metallurgical Aspects of the Stress-Corrosion Cracking of Titanium Alloys", in Fundamental Aspects of Stress-Corrosion Cracking, eds. R. W. Staehle, et al., N. A. C. E., Houston (1969), 620.

(3) M. J. Blackburn and J. C. Williams, "Strength, Deformation Modes and Fracture in Titanium-Aluminum Alloys", ASM Trans. Quart., 62, 398 (1969).

(4) R. E. Curtis, R. R. Boyer, and J. C. Williams, "Relationship Between Composition, Microstructure, and Stress-Corrosion Cracking (in Salt Solution) in Titanium Alloys", ASM Trans. Quart., 62, 457 (1969).

(5) J. L. Cavallaro and R. C. Wilcox, "Embrittlement of Ti-7Al Binary Alloy in Sea Water", Corrosion, 27, 157 (1971).

(6) J. D. Boyd and R. G. Hoagland, "The Relation Between Surface Slip Topography and Stress-Corrosion Cracking in Ti-8 Wt. % Al", Presented at the International Symposium on Stress-Corrosion Mechanisms in Ti Alloys, Atlanta, Georgia, 1971; to be published by N. A. C. E.

(7) R. A. Wood, J. D. Boyd, and R. I. Jaffee, "The Effects of Alloy Composition on the Salt-Water Stress-Corrosion Susceptibility of Titanium-Aluminum-Base Alloys", to be presented at the 2nd International Conference on Titanium, Boston, Massachusetts, May, 1972.

(8) G. Lütjering and S. Weissman, "Mechanical Properties of Age-Hardened Titanium-Aluminum Alloys", Acta Met., 18, 785 (1970).

(9) K. R. Evans, "The Embrittlement and Fracture of Ti-8 Percent Al Alloys", Trans. Aime, 245, 1297 (1969).

(10) M. J. Blackburn, "The Ordering Transformation in Titanium-Aluminum Alloys Containing up to 25 At. % Aluminum", Trans. Aime, 239, 1200 (1967).

DISTRIBUTION LIST
CONTRACT NASr-100(09)

Mr. Richard Raring
NASA Headquarters
Code RWM
Washington, D. C. 20546

Herbert F. Hardrath
SRD-Fatigue Branch
Mail Stop 129
Langley Research Center
Hampton, Virginia 23365

Eldon E. Mathauser
S.RD-Structural Materials Branch
Mail Stop 188A
Langley Research Center
Hampton, Virginia 23365

G. Mervin Ault
Materials Process Laboratory
Mail Stop 105-
Lewis Research Center
Cleveland, Ohio 44135

Albert E. Anglin, Jr.
Airbreathing Engines Div.
Mail Stop 54-
Lewis Research Center
Cleveland, Ohio 44135

Robert E. Johnson
SMD Experimental Mech
Code ES4
Manned Spacecraft Center
Houston, Texas 77058

Wilbur A. Riehl
Code R-P&VE-MC
Building 4612
Marshall Space Flight Center
Huntsville, Alabama

Charles A. Hermach
Materials Research
Mail Stop 240-1
Ames Research Center
Moffett Field, California

Naval Research Laboratory
Attn: Dr. B. F. Brown
Washington, D. C.
Code: 2300

U. S. Navy Marine Engineering
Laboratory
Alloys Division
Annapolis, Maryland 21402
Attn: Mr. W. L. Williams

Dr. Robert I. Jaffee
Battelle Memorial Institute
505 King Avenue
Columbus, Ohio 43201

Mr. Harold H. Block
Chief, Metallurgist
AiResearch Manufacturing Company
9851 Sepulveda Boulevard
Los Angeles, California

Mr. Elihu F. Bradley
Chief, Materials Engineering
Pratt & Whitney Aircraft
East Hartford, Connecticut

Prof. Mars G. Fontana
Chairman, Dept. of Metallurgical
Engineering
Ohio State University
Columbus, Ohio

Mr. Dean Hanink
Manager, Materials Laboratory
General Motors Corporation
Allison Division
Tibbs Avenue
Indianapolis, Indiana 46206

Mr. Louis P. Jahnke
Manager of Metallurgy
General Electric Corporation
Flight Propulsion Division
Cincinnati, Ohio 45215

DISTRIBUTION LIST
(Continued)

Mr. John V. Long
Director of Research
Solar Corporation
2200 Pacific Highway
San Diego, California

Dr. Alan M. Lovelace
Chief Scientist
Air Force Materials Laboratory
Wright-Patterson AFB, Ohio 45433

Mr. Ward Minkler
Manager of Technical Service
Titanium Metals Corporation of America
233 Broadway
New York, New York 10007

Mr. Winston H. Sharp
Connecticut Metallurgical Corporation
2 State Street
Hartford, Connecticut 06103

Mellon Institute
4400 Fifth Avenue
Pittsburgh, Pennsylvania
Attn: Dr. H. L. Anthony

Battelle Memorial Institute
Columbus, Ohio
Attn: Mr. Walter Boyd

Titanium Metals Corporation of America
Henderson, Nevada
Attn: Mr. H. W. Rosenberg

Reactive Metals Incorporated
Niles, Ohio
Attn: Mr. H. B. Bomberger

Crucible Steel Company of America
P. O. Box 7257
Pittsburgh, Pennsylvania 15213

Savannah River Laboratory
Nuclear Materials Division
E. I. du Pont de Nemours & Company
Aiken, South Carolina
Attn: Mr. S. P. Rideout

Materials Research Laboratory
22333 Governors Highway
Richton Park, Illinois

The Ohio State University Research Foundation
The Ohio State University
Columbus, Ohio
Attn: Prof. Franklin Beck

Douglas Aircraft Company
Newport Beach, California
Attn: Dr. N. A. Tiner

Lockheed-California Company
Box 551
Burbank, California
Attn: Mr. George Wald

National Bureau of Standards
Metallurgy Division
Washington, D. C.
Attn: Mr. Hugh Logan

Douglas Aircraft Company
Aircraft Division
Long Beach, California
Attn: Mr. R. A. Simpson

The Boeing Company
Aerospace Group
P. O. Box 3707
Seattle, Washington 98124
Attn: Dr. T. R. Beck

Dr. J. B. Arots
Research Center
Hercules, Inc.
Wilmington, Delaware 19899

North American Aviation, Inc.
Los Angeles Division
Los Angeles, California 90009
Attn: Dr. Alfred W. Sommer

Mr. William D. Klopp
Code 2351
NASA Lewis Research Center
Cleveland, Ohio 44135

DISTRIBUTION LIST
(Continued)

Mr. Carl E. Coy, Sr.
Research Engineer
The Boeing Company
Space Division, Launch
Systems Branch
P. O. Box 29100
New Orleans, Louisiana 70129

Mr. Richard D. Waltein
Materials Engineering
Hamilton Standard
Windsor Locks, Connecticut 06096

Dr. M. J. Blackburn
The Boeing Company
P. O. Box 3707
Seattle, Washington 98124

Dr. J. C. Williams
North American Rockwell Science Center
Physical Metallurgy Division
Thousand Oaks, California

Professor J. D. Embury
McMaster University
Department of Metallurgy and Materials Science
Hamilton, Ontario
Canada

Professor S. Weissmann
Rutgers University
Department of Mechanics and Materials Science
New Brunswick, New Jersey

Dr. H. L. Gegel
Air Force Materials Laboratory /LLS
Wright-Patterson Air Force Base, Ohio 45433

Dr. J. C. Scully
Department of Metallurgy
Leeds University
Leeds, England

Mr. J. L. Cavallaro
Naval Shio and Research Development Laboratory
Annapolis, Maryland

Dr. J. A. Sedriks
Research Institute for Advanced Studies
Martin Marietta Corporation
1450 South Rolling Road
Baltimore, Maryland 21227

Professor H. Margolin
Department of Metallurgy and Materials
Science
New York University
New York, N. Y. 10453

Dr. Howard G. Nelson
NASA Ames Research Center
Moffett Field, California 94035

Dr. Hugh R. Gray
NASA Lewis Research Center
Cleveland, Ohio